Spin change of a proto-neutron star by the emission of neutrinos

Chung-Yeol Ryu,[1,*] Tomoyuki Maruyama,[2,3] Toshitaka Kajino,[3,4] Grant J. Mathews,[5] and Myung-Ki Cheoun[3,6,†]

[1]*General Education Curriculum Center, Hanyang University, Seoul 133-791, Korea*

[2]*College of Bioresource Sciences, Nihon University, Fujisawa 252-8510, Japan*

[3]*National Astronomical Observatory, Mitaka, Tokyo 181-8589, Japan*

[4]*Department of Astronomy, Graduate School of Science, University of Tokyo, 7-3-1 Hongo, Tokyo 113-0033, Japan*

[5]*Center of Astrophysics, Department of Physics, University of Notre Dame, Indiana 46556, USA*

[6]*Department of Physics, Soongsil University, Seoul 156-743, Korea*

(Received 22 September 2011; revised manuscript received 16 March 2012; published 6 April 2012)

We investigate the structure of proto-neutron stars (PNSs) with trapped neutrinos by using a quark-meson coupling model. We adopt a phenomenological lepton density which is diffuse near the surface. We calculate the populations of baryons and leptons, the equations of state, and the mass-radius relation for isentropic PNS models. In addition, the moment of inertia is calculated for both PNS and cold-neutron-star (CNS) models as a means to study the change of the spin period due to the neutrino emission from a PNS. Neutrino emission from a hyperonic neutron star is shown to increase the spin by about 10% of the initial spin, while the spin of a nucleonic neutron star with a central density above $\rho_C \approx 5\rho_0$ is decreased by a few % by the emission of neutrinos. Therefore, the spin change owing to the leakage of neutrinos from a PNS is a small ($<$10%) correction compared to other processes related to the spin change.

DOI: 10.1103/PhysRevC.85.045803 PACS number(s): 25.30.Pt, 21.65.Cd, 24.10.Jv, 12.39.−x

I. INTRODUCTION

According to numerical simulations [1,2], proto-neutron stars (PNSs) are expected to be born in core-collapse supernovae (SNe) with inferred initial rotation periods of order 20–300 ms. These high initial spins are a result of angular momentum conservation, although the final spin depends upon mechanism for angular momentum transport and the spin of the progenitor star. The initial spin of a PNS may be determined from the rotation of the SN core, but the simulations tend to yield rotation periods that are either $\sim$ 1 s too slow [3] or $\sim$1 ms–15 ms, too fast [4,5] compared to observations. Therefore, some other angular-momentum transport mechanism may be in operation in outer environment of PNSs such as accretion shocks [1]. Of interest to the present work is the possibility the emission of trapped neutrinos after the SN explosion may also significantly affect the kinematics of the newly born PNSs. For example, the asymmetry of neutrino scattering and emission owing to strong internal magnetic fields may give rise to observed pulsar kicks [6]. In this work, therefore, we investigate the spin up or down of pulsars through the change of the moment of inertia caused by the neutrino emission and cooling in the evolution of PNSs.

A PNS is the early state of a neutron star produced after a core collapse SN. They are known to have trapped neutrinos within their hot and dense interiors. The evolution of a PNS involves the deleptonization of the star through the emission of neutrinos over an interval of about 20 s [7–9] after the initial core bounce. As long as neutrinos remain trapped inside a PNS, they can affect the β equilibrium. Therefore the internal structure of a PNS is altered through the influence of β equilibrium on the relative populations of baryons, the equation of state (EOS), etc.

In our previous work [10], we introduced a density dependent ratio of neutrinos in a PNS in the framework of quantum hadrodynamics (QHD) and showed that this approach is in good agreement with simulations of PNS evolution. We here extend that previous work and incorporate the modified quark-meson coupling (MQMC) model to describe a PNS with the same density dependent neutrino ratio as the previous QHD model [10]. Using the MQMC model, we describe the hot dense neutron star matter with initial conditions corresponding to those of a PNS just after a supernova core collapse. After the emission of the trapped neutrinos, the star will evolve to become a cold neutron star (CNS) at zero temperature without much change in the central density. Thus, we can study any possible changes of the rotation rate by comparing the moments of inertia of the initial PNS with models for the final CNS.

Since the quark-meson coupling (QMC) model was first proposed [11], the model has been modified [12] to recover relativistic phenomena by introducing a density dependent bag constant. This version is referred to as the modified quark-meson coupling (MQMC) model. In both the QMC and MQMC models, a nucleon is treated as a MIT bag in which quarks interact by exchanging σ, ω and ρ mesons. Both the QMC and MQMC models have been applied to finite nuclei [13], nuclear matter [12], and neutron stars [14,15].

In particular, the MQMC model benefits from the extra quark degrees of freedom. For example, the density dependence may help to explain [15] the recently observed data for PSR J1614-2230 [16] which has $M \approx 1.97 M_\odot$. As shown in our previous paper [15] and Ref. [14], the radius constraints for this star [17] agree more or less with the results obtained in the nucleonic phase of the MQMC model. In this report

*cyryu@skku.edu

†Corresponding author: cheoun@ssu.ac.kr

we calculate the structure and evolution of a PNS within the MQMC model by considering both nucleonic and hyperonic phases with trapped neutrinos.

The paper is organized as follows. In Sec. II, the MQMC model for hot and dense matter is briefly explained. Numerical results and discussions are presented in Sec. III. A summary and conclusions are given in Sec. IV.

II. THEORY

A. Models for hot dense hypernuclear matter

The total Lagrangian for hot dense matter in the mean field approximation can be represented in terms of the baryon octet, leptons and five meson fields, as follows:

$$\begin{aligned}\mathcal{L} = \sum_B \bar{\psi}_B \Big[& i\gamma\cdot\partial - M_B^*(\sigma,\sigma^*) \\ & - \gamma^0\left(g_{\omega B}\omega_0 + g_{\phi B}\phi_0 + \frac{1}{2}g_{\rho B}\tau_z\rho_{03}\right)\Big]\psi_B \\ & - \frac{1}{2}m_\sigma^2\sigma^2 - \frac{1}{2}m_{\sigma^*}^2\sigma^{*2} + \frac{1}{2}m_\omega^2\omega_0^2 \\ & + \frac{1}{2}m_\phi^2\phi_0^2 + \frac{1}{2}m_\rho^2\rho_{03}^2 + \sum_l \bar{\psi}_l(i\gamma\cdot\partial - m_l)\psi_l, \end{aligned} \tag{1}$$

where B denotes the octet of baryons and l stands for the leptons (e^-, μ^-, ν_e, ν_μ). In this work, neutrinos are regarded as left-handed and massless. Since a baryon is treated as a MIT bag in the MQMC model, the effective mass of a baryon is obtained from the MIT bag model

$$\begin{aligned} M_B^* &= \sqrt{E_B^2 - \sum_q \left(\frac{x_q}{R_B}\right)^2}, \\ E_B &= \sum_q \frac{\Omega_q}{R_B} - \frac{Z_B}{R_B} + \frac{4\pi R_B^3}{3}B_B(\sigma,\sigma^*). \end{aligned} \tag{2}$$

Here, the bag constant $B_B(\sigma,\sigma^*)$ has a density dependence as follows:

$$\begin{aligned} B_B(\sigma,\sigma^*) = B_{B0}\exp\Bigg\{ & -\frac{4}{M_B}\Bigg[g_\sigma^B \sum_{q=u,d} n_q\sigma \\ & + g_{\sigma^*}^B\left(3 - \sum_{q=u,d} n_q\right)\sigma^*\Bigg]\Bigg\}, \end{aligned} \tag{3}$$

where M_B is the mass of a baryon in vacuum and n_q is the number of quarks. The bag constant in vacuum B_{B0} and a phenomenological constant Z_B are fitted to reproduce the mass of a free baryon at a bag radius of $R_B = 0.6$ fm. Their values are taken from Ref. [15]. The quark energy, $\Omega_q = \sqrt{x_q^2 + (Rm_q^*)^2}$, is calculated from the momentum of a quark in a bag x_q of radius R and an effective quark mass of $m_q^* = m_q - g_\sigma^q\sigma - g_{\sigma^*}^q\sigma^*$. The value of x_q is determined from a boundary condition on the bag surface, $j_0(x_q) = \beta_q\, j_1(x_q)$.

The total energy density at finite temperature is then given by

$$\begin{aligned} \varepsilon = & \sum_B \frac{\gamma_B}{(2\pi)^3}\int d^3k\sqrt{k^2 + M_B^{*2}}(f_B + \bar{f}_B) \\ & + \sum_l \frac{\gamma_l}{(2\pi)^3}\int d^3k\sqrt{k^2 + m_l{}^2}(f_l + \bar{f}_l) \\ & + \frac{1}{2}m_\omega^2\omega^2 + \frac{1}{2}m_\phi^2\phi^2 + \frac{1}{2}m_\sigma^2\sigma^2 \\ & + \frac{1}{2}m_{\sigma^*}^2\sigma^{*2} + \frac{1}{2}m_\rho^2\rho^2, \end{aligned} \tag{4}$$

where the spin degeneracy factors are $\gamma_B = 2$ for baryons, $\gamma_l = 2$ for e^- and μ^-, and $\gamma_l = 1$ for neutrinos. f_B and $\bar{f}_B$ are the Fermi-Dirac distribution functions for baryons and antibaryons,

$$f_B = \frac{1}{e^{(\epsilon_B^* - \mu_B^*)/T} + 1}, \quad \bar{f}_B = \frac{1}{e^{(\epsilon_B^* + \mu_B^*)/T} + 1} \tag{5}$$

with an effective nucleon energy, $\epsilon_B^* = \sqrt{k^2 + M_B^{*2}}$, and an effective baryon chemical potential, $\mu_B^* = \mu_B - g_{\omega B}\omega - g_{\phi B}\phi - I_{Bz}g_{\rho B}\rho_{03}$ with the z-component of baryon isospin, I_{Bz}. Here, the chemical potential μ_B is determined for each baryon density ρ_B

$$\rho_B = \frac{\gamma}{(2\pi)^3}\int d^3k(f_B - \bar{f}_B), \tag{6}$$

and the ω, ϕ and ρ_{03} meson fields are obtained from ρ_B as follows:

$$\begin{aligned} \omega &= \sum_B \frac{g_{\omega B}}{m_\omega^2}\rho_B, \quad \phi = \sum_B \frac{g_{\phi B}}{m_\phi^2}\rho_B, \\ \rho_{03} &= \sum_B I_{Bz}\frac{g_{\rho B}}{m_\rho^2}\rho_B. \end{aligned} \tag{7}$$

The Fermi-Dirac distribution functions for leptons and antileptons, f_l and $\bar{f}_l$, are also given by

$$f_l = \frac{1}{e^{(\epsilon_l^* - \mu_l)/T} + 1}, \quad \bar{f}_l = \frac{1}{e^{(\epsilon_l^* + \mu_l)/T} + 1}, \tag{8}$$

where $\epsilon_l^* = \sqrt{k^2 + m_l^2}$ and $m_l = 0$ for neutrinos. The pressure is calculated from

$$\begin{aligned} P = & \sum_B \frac{1}{3}\frac{\gamma_B}{(2\pi)^3}\int d^3k\frac{k^2}{\sqrt{k^2 + M_B^{*2}}}(f_B + \bar{f}_B) \\ & + \sum_l \frac{1}{3}\frac{\gamma_l}{(2\pi)^3}\int d^3k\frac{k^2}{\sqrt{k^2 + m_l{}^2}}(f_l + \bar{f}_l) \\ & + \frac{1}{2}m_\omega^2\omega^2 + \frac{1}{2}m_\phi^2\phi^2 - \frac{1}{2}m_\sigma^2\sigma^2 \\ & - \frac{1}{2}m_{\sigma^*}^2\sigma^{*2} + \frac{1}{2}m_\rho^2\rho^2. \end{aligned} \tag{9}$$

The scalar meson fields, σ and σ^*, can be determined through a minimization of the thermodynamic potential or the maximizing of the pressure with respect to theses fields. Here, we employ the maximization of the pressure, $P(M_B^*, \sigma, \sigma^*)$.

Then the self-consistent equation for the σ meson field is

$$\frac{dP}{d\sigma} = \sum_B \left(\frac{\partial P}{\partial M_B^*}\right)_{\mu_B,T} \frac{\partial M_B^*}{\partial \sigma} + \left(\frac{\partial P}{\partial \sigma}\right)_{M_B^*} = 0. \quad (10)$$

The equation for the σ^* field can be also obtained in a similar way. The $\partial M_B^*/\partial\sigma$ in Eq. (10) is obtained from the effective mass of a baryon in the MQMC model. The entropy density is given by

$$\mathcal{S} = -\sum_i \frac{\gamma_i}{(2\pi)^3} \int d^3k [f_i \ln f_i + (1-f_i)\ln(1-f_i) + \bar{f}_i \ln \bar{f}_i + (1-\bar{f}_i)\ln(1-\bar{f}_i)], \quad (11)$$

where the summation over i includes the baryon octet and all leptons (e^-, μ^-, ν_{e^-}, ν_{μ^-}). Thus, the entropy per a baryon is given as $S = \mathcal{S}/(\sum_B \rho_B)$. In this work, all results are obtained assuming a $S = 2$ isentropic model.

B. Slowly rotating neutron stars

In this subsection, we briefly describe the moment of inertia for slowly rotating neutron stars. The details are given in Refs. [18,19]. The metric of an axially symmetric star can be written as

$$\begin{aligned} ds^2 &= g_{\mu\nu} dx^\mu dx^\nu \\ &= -e^{2\nu(r)}dt^2 + e^{2\lambda(r)}dr^2 + r^2 d\theta^2 \\ &\quad + r^2 \sin^2\theta d\phi^2 - 2\omega(r) r^2 \sin^2\theta dt d\phi \,. \end{aligned} \quad (12)$$

Here, we assume that the neutron star is rotating uniformly with a stellar frequency Ω that is well below the Kepler frequency

$$\Omega \ll \Omega_{\max} \approx \sqrt{\frac{M}{R^3}}. \quad (13)$$

In this case the slow-rotation approximation can be applied to the star. In this approximation, the moment of inertia of a uniformly rotating, axially symmetric neutron star is given by

$$I \equiv \frac{J}{\Omega} = \frac{8\pi}{3} \int_0^R r^4 e^{-\nu(r)} \frac{\bar{\omega}(r)}{\Omega} \frac{(\varepsilon(r) + P(r))}{\sqrt{1-2M(r)/r}} dr \,, \quad (14)$$

where J is the angular momentum, while $\nu(r)$ and $\bar{\omega}(r)$ are the radially-dependent metric functions. $M(r)$, $\varepsilon(r)$ and $P(r)$ are the mass of the star, energy density, and pressure, respectively. These are obtained from a solution to the Tolman-Oppenheimer-Volkoff (TOV) equation.

The metric functions $\nu(r)$ and $\lambda(r)$ in Eq. (12) are unchanged from the values of a spherically symmetric neutron star. Thus $\lambda(r)$ is simply related to the mass profile $M(r)$ by

$$g_{11}(r) = e^{2\lambda(r)} = (1 - 2M(r)/r)^{-1} \,. \quad (15)$$

$\nu(r)$ can be determined from solving a first-order differential equation, or equivalently, from evaluating the following integral:

$$\nu(r) = \frac{1}{2}\ln\left(1 - \frac{2M}{R}\right) - \int_r^R \frac{(M(x) + 4\pi x^3 P(x))}{x^2(1 - 2M(x)/x)} dx. \quad (16)$$

In the metric function, the frequency $\omega(r)$ appears as a consequence of the dragging of local inertial frames by the rotating star. The relative frequency $\bar{\omega}(r) \equiv \Omega - \omega(r)$ appearing in Eq. (14) represents the angular velocity of the fluid as measured in a local inertial reference frame. In particular, the dimensionless relative frequency $\tilde{\omega}(r) \equiv \bar{\omega}(r)/\Omega$ satisfies the following second-order differential equation:

$$\frac{d}{dr}\left(r^4 j(r) \frac{d\tilde{\omega}(r)}{dr}\right) + 4r^3 \frac{dj(r)}{dr}\tilde{\omega}(r) = 0 \,, \quad (17)$$

where

$$j(r) = e^{-\nu(r)-\lambda(r)} = e^{-\nu(r)}\sqrt{1-2M(r)/r} \quad \text{if} \quad r \leqslant R \,, \qquad 1 \quad \text{if} \quad r > R \,. \quad (18)$$

Note that $\tilde{\omega}(r)$ is subject to the following two boundary conditions:

$$\tilde{\omega}'(0) = 0 \,, \quad (19)$$

$$\tilde{\omega}(R) + \frac{R}{3}\tilde{\omega}'(R) = 1 \,. \quad (20)$$

Also note that in the slow-rotation approximation, the moment of inertia does not depend on the stellar frequency Ω. In practice, one chooses an arbitrary value for the central frequency $\tilde{\omega}_c = \tilde{\omega}(0)$ and numerically integrates Eq. (17) up to the edge of the star. In general, the boundary condition at the surface, Eq. (20), will not be satisfied for an arbitrary choice of $\tilde{\omega}_c$, so one must rescale the function and its derivative by an appropriate constant to correct the mismatch.

The moment of inertia can be calculated from an integration of the equations described above. After solving for both $\tilde{\omega}(r)$ and I, one can check the consistency of the solution by how well is satisfies following condition:

$$\tilde{\omega}'(R) = \frac{6I}{R^4} \,. \quad (21)$$

C. Conditions of a PNS with trapped neutrinos

Neutron star structure is usually constrained by three conditions: (1) baryon number conservation; (2) charge neutrality; and (3) β (chemical) equilibrium. For a PNS with trapped neutrinos, however, the β chemical equilibrium has to be modified with the chemical potential due to the trapped neutrinos, μ_ν, as follows:

$$\begin{aligned} &\mu_n = \mu_p + \mu_e - \mu_\nu, \quad \mu_{\Sigma^+} = \mu_p, \\ &\mu_\Lambda = \mu_{\Sigma^0} = \mu_{\Xi^0} = \mu_n, \quad \mu_{\Sigma^-} = \mu_{\Xi^-} = \mu_n + \mu_e - \mu_\nu. \end{aligned} \quad (22)$$

In chemical equilibrium, the matter becomes symmetric matter if $\mu_e = \mu_\nu$. To allow for the dependence of the neutrino propagation and β equilibrium on density and temperature, we assume that the density of electron neutrinos can be related to the electron density, i.e., $\rho_{\nu_e} = x(\rho)\rho_e$. The condition for muon production is also taken as $\rho_{\nu_\mu} = x(\rho)\rho_\mu$ by satisfying the chemical equilibrium $\mu_e + \mu_{\nu_e} = \mu_\mu + \mu_{\nu_\mu}$. In general, $x(\rho)$ may depend on both baryon density and temperature. However, for simplicity in our previous work [10], we proposed a

phenomenological formula depending only on the baryon density,

$$x(\rho) = x_0[1 - \exp\{-\beta\,(\rho/\rho_0)^\gamma\}], \tag{23}$$

with $x_0 = 0.3$, $\beta = 0.05$ and $\gamma = 2$ [10]. The coupling constants are taken from Ref. [20].

III. RESULTS AND DISCUSSIONS

The relative populations of particles in both nucleonic and hyperonic phases are shown in Fig. 1. Results from the MQMC model show a behavior similar to our previous work based upon the QHD model [10]. In the nucleonic phase [(a) and (b)], the effect of trapped neutrinos appears as the increase of protons by the modified beta equilibrium in Eq. (22). For the hyperonic phase [Figs. 1(a) and 1(b)] the presence of trapped neutrinos causes the fraction of protons to be larger and suppresses specific charged hyperons in order to maintain baryon number conservation and charge neutrality. Neutrons are also decreased in both phases because of the increased abundance of protons.

In Fig. 2, the ratio of trapped electron neutrinos is shown for both nucleonic and hyperonic phases. For symmetric and asymmetric matter (or neutron star matter), both the QHD and MQMC models show quite similar behavior for the nucleonic and hyperonic phases [15]. For the proto-neutron star models taking account of temperature effects, the neutrino populations from the MQMC model are also similar to the results from our previous QHD work [10]. The population of electron neutrinos obtained by our density dependent ratio of trapped neutrinos agrees well with that of the transport theory simulation of Refs. [7,9]. In particular, the electron-neutrino fraction $Y_{\nu_e} \approx$ 0.06–0.07 at high densities in the np phase obtained in the simulation is similar to the result denoted by the red curve in Fig. 2.

Therefore, populations of particles including neutrinos in a PNS are well described by the density dependent neutrino model, independently of whether the QHD or MQMC model is employed. Notice, however, that according to our calculations, the neutrino population in the hyperonic phase can reduce to half of that of the np phase.

The upper panel in Fig. 3 shows the effects of trapped neutrinos on the equation of state (EOS) for both phases. In β equilibrium, $\mu_n = \mu_p + \mu_e - \mu_\nu$, trapped neutrinos make the fraction of protons higher. As a result, the star at high densities becomes nearly symmetric matter having the same ratio of neutrons and protons, as shown in Fig. 1. Thus, in the np phase, trapped neutrinos cause the EOS to be softer than the np phase without neutrinos. On the contrary, for hyperonic matter, hyperons and protons may be increased by the trapped neutrinos from the the chemical equilibrium in Eq. (22). The increased protons, however, suppress hyperons by baryon number conservation. One should keep in mind that increased protons make the $npH\nu$ EOS softer, but the suppression of hyperons makes the EOS stiffer. Because the effect of suppressed hyperons is larger than that of increased protons, the EOS for the $npH\nu$ gas becomes stiffer than that of the npH EOS.

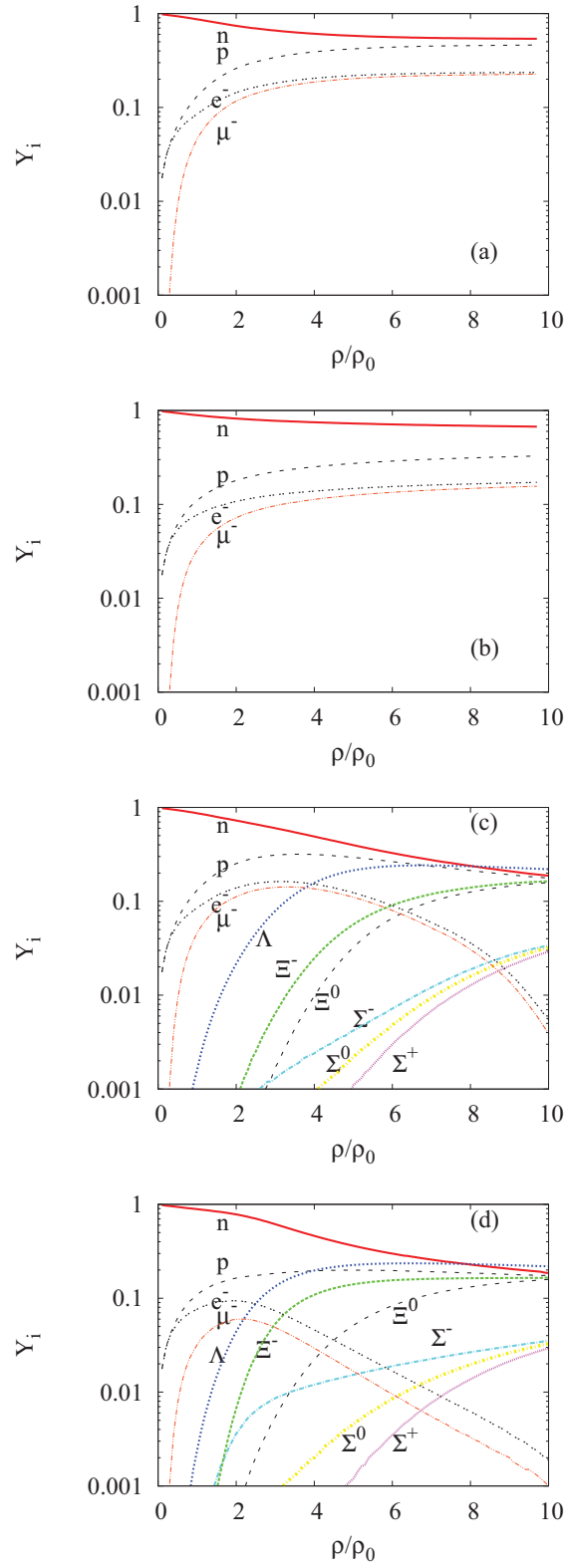

FIG. 1. (Color online) Populations of particles in nucleonic phase [(a) and (b)] and hyperonic one [(c) and (d)]. Effects of trapped neutrinos are included in (a) and (c) while (b) and (d) are results without neutrinos.

The temperature profile is shown in the lower panel of Fig. 3 for nontrapped (np and npH) and trapped cases

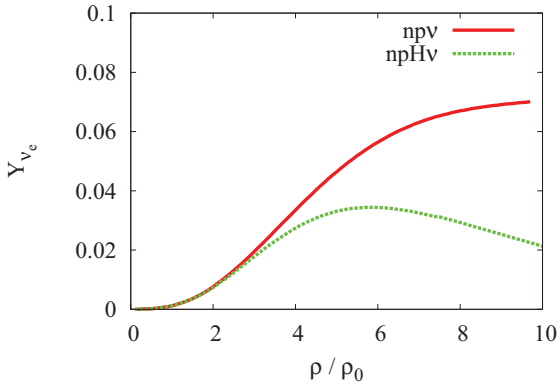

FIG. 2. (Color online) Population of electron neutrinos in both nucleonic and hyperonic phases.

$(npν)$ and $(npHν)$ based upon our density dependent $Y_{Le}(\rho)$. To keep the entropy $(S = 2)$ constant, the np phase needs higher temperature than the $npν$ phase. This is because the high temperature must compensate the increased entropy due to the trapped neutrinos. On the contrary, in hyperonic matter, the trapped neutrinos do not affect the temperature profile much because the additional hyperons also make the entropy larger for a fixed temperature.

The mass radius relation for various hot PNS models with and without neutrino trapping are shown in the upper panel of Fig. 4. These were obtained by solving the TOV equation.

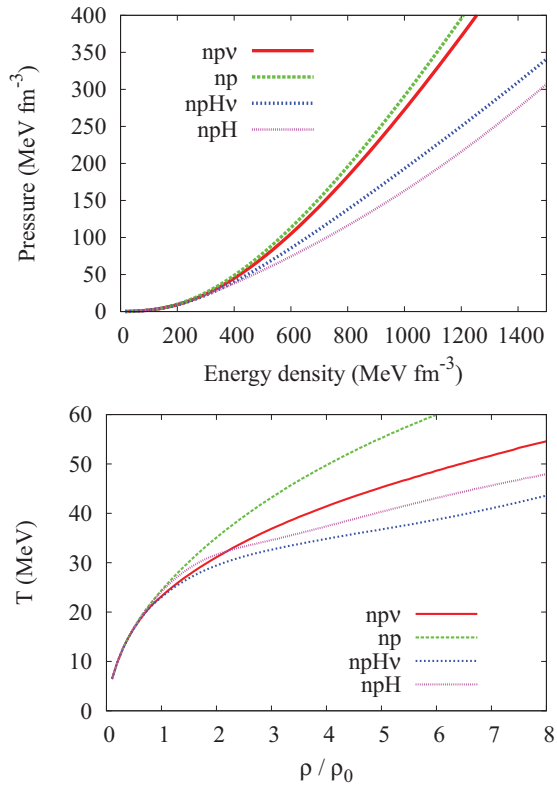

FIG. 3. (Color online) The equations of state and temperature profile for nontrapped (np and npH) and trapped cases ($npν$ and $npHν$).

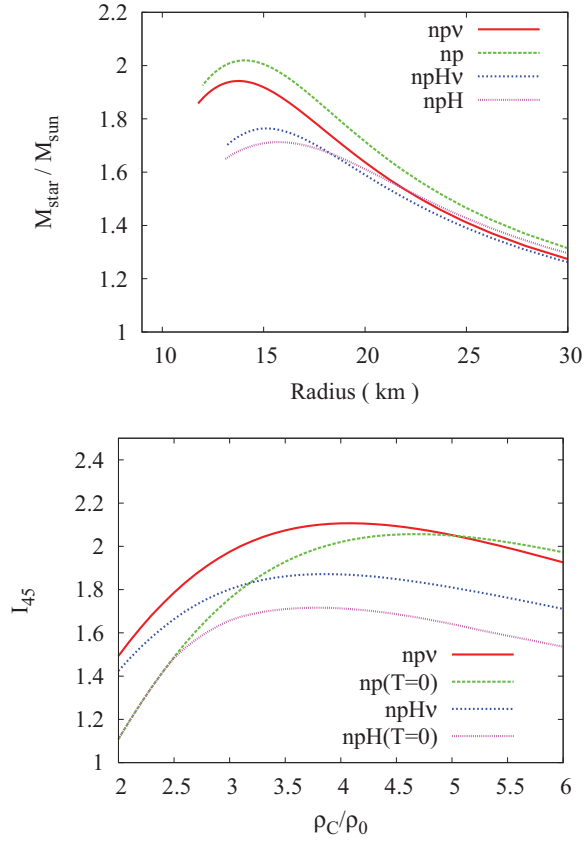

FIG. 4. (Color online) The mass radius relation and the moment of inertia for various hot PNS models.

For comparison, Fig. 5 shows the mass radius relation for cold neutron star models based upon the nucleonic and hyperonic equations of state. A good figure of merit for an equation of state is the radius of a cold neutron star of 1.4 $M_\odot$. For both the nucleonic and hyperonic equations of state we obtain a radius of 13 km for a 1.4 $M_\odot$ star. This is consistent with existing observations (e.g., $R = 12 \pm 1$ [21]) and other equations of state (e.g., [17]). We note, however, that our hyperonic EOS cannot accommodate the observed neutron star mass of $M \approx 1.97 M_\odot$ for PSR J1614-2230 [16]. However, it is a well known

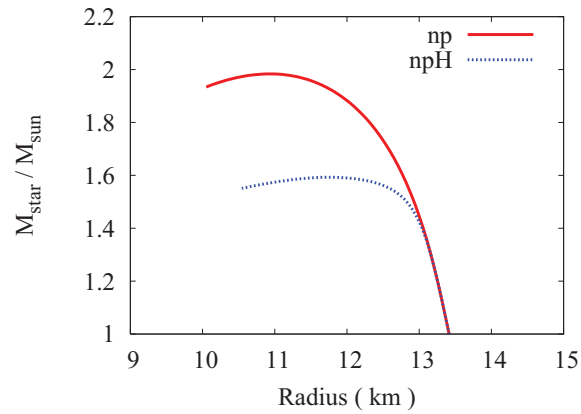

FIG. 5. (Color online) The mass-radius relation for cold neutron star models.

[17] that this problem can be fixed by the introduction of a repulsive three-body force at high density.

For the PNS models with the nucleonic EOS (np and $np\nu$), the trapped neutrinos ($np\nu$) reduce the mass for a star of fixed radius by about $0.1M_\odot$. This is because the $np\nu$ EOS is softer than that of np matter alone. However, in the hyperonic EOS (npH and $npH\nu$) the situation is a bit more complicated. Beyond the maximum mass $\sim 1.7M_\odot$, trapped neutrinos increase the mass at fixed radius by about $0.1M_\odot$, while the mass of stars for the $npH\nu$ EOS below the maximum mass are smaller for fixed radii than that of the npH EOS because of the contribution from protons. As mentioned above, the EOS becomes softer as the protons increase and stiffer by the hyperon suppression. Therefore, if we choose a very high central density where the effects of the hyperon suppression are easily expected, the mass of the $npH\nu$ models may be slightly larger those based upon the npH EOS. It is worthwhile to note the comparison of our present models to the previous QMC models of [14]. The np and npH phase models used here simply correspond to the "np" and QMC II model of Ref. [14], respectively. Of course, both results for the mass-radius relation by the present and previous calculations are well matched to each other.

Finally, we discuss the effects of trapped neutrinos on the moment of inertia by comparing the results of trapped neutrinos in a PNS with those for a cold neutron star (CNS) calculated from the equation of state in Ref. [15]. The lower panel of Fig. 4 shows that the moment of inertia usually decreases by about 10% by the neutrino emission. Consequently, the spin of the PNS is increased and the spin period is decreased by such an amount at the stage of a CNS. This feature is consistent with the following conjecture. Since the effect of temperature makes the radius of a PNS increase, the moment of inertia in PNS models ($I \sim MR^2$) is larger than that of CNS models.

However, in the central density region above $\rho_C \approx 5\rho_0$ of the np phase, the situation may be changed. One can see an interesting behavior, i.e., the moment of inertia for the nucleonic PNS phase may increase in the CNS phase by the neutrino emission. This is because the maximum mass of a CNS may be larger than that of a PNS as shown at the mass-radius relations in upper figure. The moment of inertia of the CNS becomes larger in the high central density region above $\rho_C \approx 5\rho_0$.

On the contrary, in the hyperonic phase, the moment of inertia of the PNS stage is reduced by $\approx 0.1I_{45}$ at the CNS stage, independently of the central density. Thus, if the neutron star has a hyperonic phase in the core, the initial spin may be increased about 10% by the neutrino emission.

For the np phase, however, the spin up or not depends upon the central density. Namely, the spin change ratio may depend on the mass of the relevant neutron star. Therefore, the stars with a np phase in the core may show either spin up or spin down by the neutrino emission. Which is the more plausible of the two possibilities is closely associated with the central density of the np phase of the neutron stars. However, the amount of the spin change should be less than about 10%, irrespective of the related phases of the neutron stars.

IV. SUMMARY

We have studied the effects of trapped neutrinos on a PNS by using an MQMC model. The probability of neutrino trapping is assumed to depend on the matter density. With those assumptions, we calculated the populations of relevant particles, the EOS, and the mass-radius relation of isentropic PNS models for both nucleonic and hyperonic neutron stars. We find that the emission of neutrinos decreases the moment of inertia in both phases, and hence, can make both nucleonic and hyperonic neutron stars spin up by as much as 10% of their initial spin. The spin up in the massive nucleonic phase with high central density, however, could be reversed into a spin down.

During core-collapse SNe, the angular momentum can be transported by the convection stemming from the mass accretion shock or carried away by gravitational radiation. The change in spin due to the leakage of neutrinos from a PNS can be a small correction compared to other processes. Nevertheless, although the correction is relatively small, a more thorough analyses of the relation between spin periods and neutron-star star masses may be necessary steps to better understand the spin distribution of proto-neutron stars.

ACKNOWLEDGMENTS

This work was supported by the National Research Foundation of Korea (2011-0003188 and 2011-0015467). Work at NAOJ was supported in part by Grants-in-Aid for Scientific Research of JSPS (21540412, 20244035) and Scientific Research on Innovative Area of MEXT (20105004), and also by Heiwa Nakajima Foundation. Work at the University of Notre Dame (G.J.M.) supported by the US Department of Energy under Nuclear Theory Grant No. DE-FG02-95-ER40934.

[1] J. M. Blondin and A. Mezzacappa, Nature **445**, 58 (2007).
[2] C. A. Faucher-Giguere and V. M. Kaspi, Astrophys. J. **643**, 332 (2006).
[3] H. Spruit and E. S. Phinney, Nature **393**, 139 (1998).
[4] C. D. Ott, A. Burrows, T. A. Thompson, E. Livne, and R. Walder, Astrophys. J. Suppl. **164**, 130 (2006).
[5] A. Heger, S. E. Woosley, and H. C. Spruit, Astrophys. J. **626**, 350 (2005).
[6] Tomoyuki Maruyama, Toshitaka Kajino, Nobutoshi Yasutake, Myung-Ki Cheoun, and Chung-Yeol Ryu, Phys. Rev. D **83**, 081303(R) (2011).
[7] A. Burrows and J. M. Lattimer, Astrophys. J. **307**, 178 (1986).

[8] M. Prakash, I. Bombaci, M. Prakash, P. J. Ellis, J. M. Lattimer, and R. Knorren, Phys. Rep. **280**, 1 (1997).
[9] J. A. Pons, S. Reddy, M. Prakash, J. M. Lattimer, and J. A. Miralles, Astrophys. J. **513**, 780 (1999).
[10] C. Y. Ryu, T. Maruyama, T. Kajino, and M. K. Cheoun, Phys. Rev. C **83**, 018802 (2011).
[11] P. A. M. Guichon, Phys. Lett. B **200**, 235 (1988).
[12] X. Jin and B. K. Jennings, Phys. Rev. C **54**, 1427 (1996).
[13] K. Saito, K. Tsushima, and A. W. Thomas, Nucl. Phys. A **609**, 339 (1996).
[14] S. Pal, M. Hanauske, I. Zakout, H. Stocker, and W. Greiner, Phys. Rev. C **60**, 015802 (1999).
[15] C. Y. Ryu, C. H. Hyun, S. W. Hong, and B. T. Kim, Phys. Rev. C **75**, 055804 (2007).
[16] P. B. Demorest, T. Pennucci, S. M. Ransom, M. S. E. Roberts, and J. W. T. Hessels, Nature **467**, 1081 (2010).
[17] K. Hebeler, J. M. Lattimer, C. J. Pethick, and A. Schwenk, Phys. Rev. Lett. **105**, 161102 (2010).
[18] N. K. Glendenning, *Compact Stars* (Springer-Verlag, New York, 2000).
[19] F. J. Fattoyev and J. Piekarewicz, Phys. Rev. C **82**, 025810 (2010).
[20] I. Zakout, W. Greiner, and H. R. Jaqaman, Nucl. Phys. A **759**, 201 (2005).
[21] S. Guillot, R. E. Rutledge, and E. F. Brown, Astrophys. J. **732**, 88 (2011).